A Computational study of pyrazinamide: tautomerism, acid-base properties, micro-solvation effects and acid hydrolysis mechanism

ARTICLE *in* COMPUTATIONAL AND THEORETICAL CHEMISTRY · JULY 2014

Impact Factor: 1.55 · DOI: 10.1016/j.comptc.2014.07.013

4 AUTHORS:

Mwadham M Kabanda
North West University South Africa
46 PUBLICATIONS **538** CITATIONS
SEE PROFILE

Van Tan Tran
chemistry
15 PUBLICATIONS **96** CITATIONS
SEE PROFILE

Quoc Tri Tran
Dong Thap University
4 PUBLICATIONS **8** CITATIONS
SEE PROFILE

Eno Ebenso
North West University South Africa
80 PUBLICATIONS **333** CITATIONS
SEE PROFILE

Chemical Physics Letters 627 (2015) 121–125

Contents lists available at ScienceDirect

Chemical Physics Letters

journal homepage: www.elsevier.com/locate/cplett

On the multi-reference character of the low-lying states of the $MnS^{-/0}$ clusters by the NEVPT2 assignment of the anion photoelectron spectrum

Van Tan Tran [a], Quoc Tri Tran [a], Marc F.A. Hendrickx [b,*]

[a] Theoretical and Physical Chemistry Division, Dong Thap University, 783-Pham Huu Lau, Cao Lanh City, Dong Thap, Viet Nam
[b] Afdeling Kwantumchemie en Fysicochemie, Departement Chemie, Katholieke Universiteit Leuven, Celestijnenlaan 200F, B-3001 Heverlee-Leuven, Belgium

ARTICLE INFO

Article history:
Received 27 February 2015
In final form 24 March 2015
Available online 1 April 2015

ABSTRACT

Low-lying electronic states of the $MnS^{-/0}$ clusters have been investigated by DFT, RCCSD(T), and NEVPT2 methods. The anionic ground state is predicted to be $^7\Sigma^+$ while the neutral ground state is confirmed as $^6\Sigma^+$. The $^7\Sigma^+ \rightarrow {}^6\Sigma^+$ transition is proposed to be at the origin of the lowest energy band of the anion photoelectron spectrum. The $^7\Sigma^+ \rightarrow {}^6\Pi$ transition is demonstrated to be responsible for the higher energy band. The Franck–Condon factor simulations for these two ionizations, as based on the NEVPT2 potential energy curves, confirm the experimental broadness of the two bands.

1. Introduction

It is a well-known fact that numerous vital biochemical and economically important industrial processes depend on transition metal sulfide clusters as catalysts [1,2]. Consequently, these clusters are widely and intensely investigated by both theoretical and experimental chemists. In particular, matrix-isolation infrared spectroscopy was applied successfully to characterize many stable isomers [3–7]. Also, photoelectron spectroscopy was employed to probe the geometrical and electronic structures of iron-sulfur $FeS_n^{-/0}$ (n = 1–6) and manganese–sulfur $Mn_nS_m^{-/0}$ (n = 1–10, m = 1–10) clusters [8–10]. Due to frequent near-degeneracy of low-lying electronic states and equal stability of different isomers of a specific stoichiometric cluster, the $FeS_n^{-/0}$ (n = 1–4) clusters were studied with multi-reference wave function methods such as multi-reference configuration interaction (MRCI) and complete active space second-order perturbation theory (CASPT2). Especially, the CASPT2 method, with an ability to calculate all low-lying electronic states for an acceptable computational cost, was used to afford assignments for the photoelectron spectra of FeS_n^- (n = 1–4) [11–14]. When necessary, various DFT and RCCSD(T) methods were applied to identify the most stable isomers and ground states of these clusters [13,14].

Due to their complex electronic structures the application of quantum chemical methods to manganese–sulfur clusters is rather limited. DFT is the most common method employed to study manganese–sulfur clusters because of its low computational cost. The small to medium sized manganese–sulfur clusters, such as clusters ranging from MnS_2 to $Mn_{15}S_{15}$ [15] and MnS_x^+ (x = 1–10) [16], were investigated with DFT. Surprisingly, for the smallest stoichiometric $MnS^{-/0}$ clusters, there are no DFT data available in the literature. On the other hand, the multi-reference wave function MCPF (modified coupled-pair function approach) and single-reference wave function CCSD(T) methods were employed to study only the neutral MnS cluster. The results showed that the ground state of the neutral cluster is a $^6\Sigma^+$ [17]. To the best of our knowledge there is no investigation carried out so far on the anionic cluster. Moreover, the anion photoelectron spectrum is not fully understood although it was reported in the literature a long time ago [10]. An assignment of the anion photoelectron spectrum of the MnS^- cluster was made based on a previous computational study of the neutral MnS cluster [10]. The lowest energy band (denoted as X in this contribution) was assigned as the transition to the neutral $^6\Sigma^+$ ground state, while the higher energy band (denoted as A in this contribution) was ascribed to the transition to the neutral $^4\Pi$ first excited state. This assignment means that the anionic ground state should be a quintet according to the spin selection rule of photoelectron spectroscopy. However, this anionic quintet ground state is not confirmed by any quantum chemical calculation. From the computational approaches applied to the $FeS_n^{-/0}$ clusters [11–14], we can deduce that each adequate investigation of the electronic structures of $MnS^{-/0}$ clusters needs to be carried out with multi-reference methods. At the present, we are interested in the performance of the NEVPT2 (N-Electron Valence

* Corresponding author.
E-mail address: marc.hendrickx@chem.kuleuven.be (M.F.A. Hendrickx).

http://dx.doi.org/10.1016/j.cplett.2015.03.049
0009-2614/

Table 1
Adiabatic and vertical relative energies (AREs and VREs), bond distances, harmonic vibrational frequencies, and electronic leading configurations of the low-lying states of $MnS^{-/0}$ as calculated with NEVPT2. VREs were obtained based on the geometry of the $^7A_1$ ($^7\Sigma^+$).

Cluster	State	Leading configuration	Weight	Mn–S	Freq.	ARE (eV)			VRE (eV)		
			(%)	(Å)	(cm^{-1})	AS I	AS II	Expt.	AS I	AS II	Expt.
MnS^-	$^7A_1$ ($^7\Sigma^+$)	$10a_1^2 11a_1^1 12a_1^1 13a_1^1 4b_1^2 5b_1^1 4b_2^2 5b_2^1 1a_2^1$	96	2.169	438	0.00	0.00		0.00	0.00	
	$^5A_1$ ($^5\Sigma^+$)	$10a_1^2 11a_1^1 12a_1^2 13a_1^0 4b_1^2 5b_1^1 4b_2^2 5b_2^1 1a_2^1$	43	2.121	413	0.39			0.41		
	$^5B_1$ ($^5\Pi$)	$10a_1^2 11a_1^1 12a_1^1 13a_1^2 4b_1^2 5b_1^0 4b_2^2 5b_2^1 1a_2^1$	45						1.59		
	$^5A_2$ ($^5\Delta$)	$10a_1^2 11a_1^1 12a_1^0 13a_1^2 4b_1^2 5b_1^1 4b_2^2 5b_2^1 1a_2^2$	44						2.71		
MnS	$^4B_1$ ($^4\Pi$)	$10a_1^2 11a_1^1 12a_1^0 13a_1^2 4b_1^2 5b_1^0 4b_2^2 5b_2^1 1a_2^1$	25						2.87		
	$^6A_1$ ($^6\Sigma^+$)	$10a_1^2 11a_1^1 12a_1^1 13a_1^0 4b_1^2 5b_1^1 4b_2^2 5b_2^1 1a_2^1$	90	2.038	461	1.57	1.63	1.77	1.67	1.75	2.03
	$^6B_1$ ($^6\Pi$)	$10a_1^2 11a_1^1 12a_1^1 13a_1^1 4b_1^2 5b_1^0 4b_2^2 5b_2^1 1a_2^1$	42	2.264	352	2.33	2.58		2.37	2.62	2.78
	$^8B_1$ ($^8\Pi$)	$10a_1^2 11a_1^1 12a_1^1 13a_1^1 4b_1^1 5b_1^1 4b_2^2 5b_2^1 1a_2^1$	98	2.344	360	2.45	2.70		2.63	2.88	

State Pertubation Theory) computational technique. Indeed, this method uses a more advanced zeroth-order Hamiltonian (the Dyall Hamiltonian) than CASPT2, which renders it size consistent and intruder state free [18–20]. Recently, benchmark calculations concerning vertical excitation energies of organic molecules show that NEVPT2 exhibits a similar accuracy compared to CASPT2 [21]. Further, this relatively new method was also applied to investigate many properties of transition metal-containing clusters and complexes [22–26]. For all these reasons, NEVPT2 calculations will be carried out in this work to study the electronic structures of the $MnS^{-/0}$ clusters. Based on these computational results, we will demonstrate that it is possible to make assignments for bands of the photoelectron spectrum of MnS^-. DFT and RCCSD(T) methods were also applied with the purpose to find out how they perform in comparison to NEVPT2 for these clusters.

2. Computational methods

Three different methods including DFT, RCCSD(T), and NEVPT2 were applied in the search for the minima of the potential energy curves and the relative stabilities, and to evaluate the harmonic vibrational frequencies for all low-lying electronic states of the $MnS^{-/0}$ clusters. All DFT calculations were carried out in a spin unrestricted way by ORCA 3.01 [27]. Both pure BP86 [28,29] and hybrid B3LYP [28,30,31] functionals were utilized in combination with the def2-QZVP basis set [32]. The RCCSD(T) calculations were done with the MOLPRO 2009 computer programs [33] based on the restricted open-shell Hartree–Fock (ROHF) wave functions. The aug-cc-pwCVTZ-DK [34] and aug-cc-pVTZ-DK basis sets [35] were employed for Mn and S, respectively. Electrons in the 3s, 3p, 3d, and 4s orbitals of Mn and in 3s and 3p orbitals of S were correlated in the RCCSD(T) calculations.

NEVPT2 calculations were performed with the DALTON 2011 [36,37] suite of programs. The orbitals needed were obtained from CASSCF calculations, for which two sets of active space orbitals were employed. The smallest active space (AS I) includes the 3d and 4s orbitals of Mn and the 3p and 4p orbitals of S. This results in an active space of 11 and 12 electrons in 12 orbitals with 5 orbitals of a_1, 3 orbitals of b_1, 3 orbitals of b_2, and 1 orbital of a_2 symmetry. A second larger active space (AS II) was formed by adding 1 orbital of a_1, 1 orbital of b_1, and 1 orbital of b_1 symmetry to AS I. The resulting larger active space has 11 and 12 elections distributed among 15 orbitals. AS I was used with the aug-cc-pVTZ-DK basis set [35] to derive the Mn–S bond distances and harmonic vibrational frequencies, while AS II was utilized with the aug-cc-pVQZ-DK [35] basis set for single-point calculations in order to improve the relative energies. Electrons in the 1s, 2s, and 2p orbitals of Mn and S were not correlated in the perturbation step.

Scalar-relativistic effects were included in RCCSD(T) and NEVPT2 calculations through the second-order Douglas–Kroll Hamiltonian [38–40]. Although $MnS^{-/0}$ clusters possess $C_{\infty v}$ symmetry, our calculations were performed by using C_{2v} symmetry, since only Abelian point groups are supported in the employed computer codes. In order to reproduce the bandwidths of the two low-lying bands in the experimental anion photoelectron spectrum of MnS^-, Franck–Condon factor simulations were performed. For this purpose NEVPT2 potential energy curves were constructed manually, from which the necessary equilibrium bond lengths and harmonic vibrational frequencies of the relevant electronic states were derived.

3. Results and discussion

3.1. The low-lying states of $MnS^{-/0}$

Based on the NEVPT2 results several low-lying electronic states for the $MnS^{-/0}$ clusters are reported in Table 1. As can be seen, the adiabatic relative energies (AREs) and vertical relative energies (VREs) only slightly increase from active space I to active space II. Since the active space I was employed for all the needed low-lying states, our discussion on the relative stability of low-lying states mainly uses these results. For the first time ever, the anionic ground state is calculated to be the $^7A_1$ ($^7\Sigma^+$) with an equilibrium Mn–S bond length of 2.169 Å. The first excited state of the anionic cluster, labeled as $^5A_1$ ($^5\Sigma^+$), with a bond distance of 2.121 Å is placed at 0.39 eV above the ground state. Additionally, at higher energy, our results also locate a $^5B_1$ ($^5\Pi$) and a $^5A_2$ ($^5\Delta$) with vertical relative energies of 1.59 eV and 2.71 eV, respectively. For the neutral cluster, NEVPT2 confirms the previous study [17], and predicts the $^6A_1$ ($^6\Sigma^+$) as the lowest energy state with a bond distance of 2.038 Å. Above this neutral ground state at 0.76 eV and 0.88 eV, the $^6B_1$ ($^6\Pi$) first excited and the $^8B_1$ ($^8\Pi$) second excited state were located, with Mn–S bond distances amounting to 2.264 Å and 2.344 Å, respectively. The lowest quartet states, which was previously believed to be responsible for the A band in the experimental spectrum, turns out to the $^4B_1$ ($^4\Pi$) state. It is calculated to be as much as 1.2 eV higher than the neutral ground states, as determined from the calculated vertical relative energies.

With the knowledge of the CASSCF electronic leading configurations, DFT calculations were also carried out for the relevant

Table 2
Relative energies, bond distances, and harmonic vibrational frequencies for the low-lying states of $MnS^{-/0}$ as calculated at the DFT and RCCSD(T) levels.

Method	Cluster	State	Mn–S (Å)	Freq. (cm^{-1})	RE (eV)
B3LYP	MnS^-	$^7A_1$ ($^7\Sigma^+$)	2.180	431	0.00
		$^5A_1$ ($^5\Sigma^+$)	2.137	429	0.04
	MnS	$^6A_1$ ($^6\Sigma^+$)	2.067	495	1.55
		$^6B_1$ ($^6\Pi$)	2.293	355	2.50
		$^8B_1$ ($^8\Pi$)	2.381	333	2.65
BP86	MnS^-	$^7A_1$ ($^7\Sigma^+$)	2.147	439	0.00
		$^5A_1$ ($^5\Sigma^+$)	2.086	455	0.10
	MnS	$^6A_1$ ($^6\Sigma^+$)	2.040	511	1.52
		$^6B_1$ ($^6\Pi$)	2.213	344	2.86
		$^8B_1$ ($^8\Pi$)	2.353	336	3.10
RCCSD(T)	MnS^-	$^7A_1$ ($^7\Sigma^+$)	2.183	434	0.00
	MnS	$^6A_1$ ($^6\Sigma^+$)	2.072	487	1.96

low-lying states. The corresponding results are presented in Table 2. Similar to NEVPT2, both B3LYP and BP86 functionals are able to confirm the $^7A_1$ ($^7\Sigma^+$) and $^6A_1$ ($^6\Sigma^+$) anionic and neutral ground states. For the anionic $^5A_1$ ($^5\Sigma^+$) first excited state, B3LYP and BP86 give relative energies of 0.04 and 0.10 eV, respectively, which are erroneously much smaller than the value of 0.39 eV as obtained by NEVPT2. These too low relative energies of $^5A_1$ ($^5\Sigma^+$) as obtained by DFT can be explained by the strong multi-reference character of this state. As can see in Table 1, its reference weight of the leading configuration is only 43%. Otherwise, the first excited state of the neutral cluster is still predicted as the $^6B_1$ ($^6\Pi$) which is located at 0.95 and 1.34 eV above the neutral ground states by B3LYP and BP86 functionals. Also, the second excited state is computed as the $^8B_1$ ($^8\Pi$) by B3LYP and BP86 functionals with relative energies compared to the neutral ground state of 1.10 and 1.58 eV. In general, we can state that DFT confirms the NEVPT2 relative energy order of the low-lying states of $MnS^{-/0}$ although the $^5A_1$ ($^5\Sigma^+$) of the anionic cluster is erroneously stabilized by DFT due to the strong multi-reference character of its wave function.

The NEVPT2 and DFT results allow to conclude that the anionic ground state is definitely the $^7A_1$ ($^7\Sigma^+$) state which consequently should be used as the initial state for the electron detachments observed in the anion photoelectron spectrum. This fact will lead to a novel assignment of the spectrum, because in the previous study [10], the X and A bands were tentatively assigned to the $^6\Sigma^+$ and $^4\Pi$, meaning that the anionic cluster must have a quintet ground state according to the spin selection rule of photoelectron spectroscopy. Tables 1 and 2 further allow to conclude that without any doubt the neutral ground and first excited states are $^6A_1$ ($^6\Sigma^+$) and $^6B_1$ ($^6\Pi$), respectively. Therefore, the photoelectron spectrum of MnS^- needs to be re-interpreted with the new computational results. Vice versa, the experimental binding energies permit to evaluate critically the applicability and accuracy of the various employed computational techniques.

3.2. *Electronic structures of $MnS^{-/0}$*

For the assignment of the photoelectron spectrum a knowledge of the orbital occupancies of the initial anionic and low-lying neutral states is of vital importance. The necessary electronic structures of the low-lying states of $MnS^{-/0}$ are identified from the CASSCF electronic leading configurations as presented in Table 1. For the anionic $^7A_1$ ($^7\Sigma^+$) ground state, as can be seen in Figure 1, all the predominantly manganese valence orbitals, including the d_δ ($11a_1$, $1a_2$), d_σ ($12a_1$), d_π ($5b_1$, $5b_2$), and 4s,4p ($13a_1$), are all singly occupied. The predominantly 3p orbital of sulfur, containing the p_σ ($10a_1$) and p_π ($4b_1$, $4b_2$), are all doubly occupied. This is in agreement with the classical electronic structure picture for this type

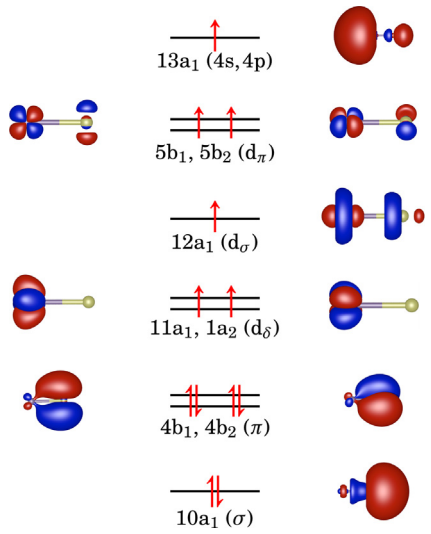

Figure 1. Qualitative molecular orbital diagram depicting the CASSCF pseudo-natural orbitals and their occupation in the leading configuration of the $^7A_1$ ($^7\Sigma^+$) ground state of MnS^-. The manganese nucleus is situated at the left hand side of the orbital plots.

of singly coordinated unsaturated transition metal complexes, in which the valence ligand orbitals are closed shell lower lying σ or π bonding orbitals. The dominant valence metal orbitals on the other hand are the higher positioned σ anti-bonding ($12a_1$), the π anti-bonding orbitals ($5b_1$ and $5b_2$), or the predominantly nonbonding δ orbitals ($11a_1$, $1a_2$). Also rather typically [12,41] and because of the low-lying 4s orbital, there is an additional nonbonding orbital of σ symmetry ($13a_1$), which pushes the $12a_1$ downwards. The neutral $^6A_1$ ($^6\Sigma^+$), $^6B_1$ ($^6\Pi$), and $^8B_1$ ($^8\Pi$) states are obtained by the detachment of an electron from the 4s, d_π, and p_π orbitals, respectively. Also, our CASSCF results in Table 1 show that the wave functions of the $^5A_1$ ($^5\Sigma^+$), $^5B_1$ ($^5\Pi$), $^5A_2$ ($^5\Delta$), $^4B_1$ ($^4\Pi$), and $^6B_1$ ($^6\Pi$) states have pronounced multi-reference character. The reference weights of the CASSCF electronic leading configurations of these states have

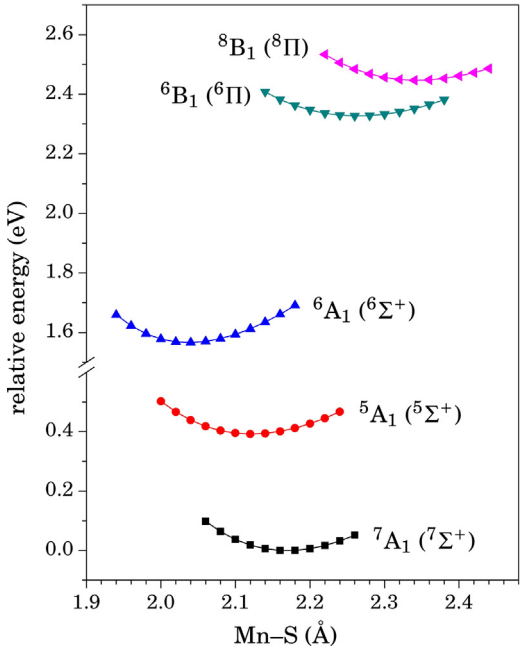

Figure 2. NEVPT2 potential energy curves for the low-lying states of $MnS^{-/0}$.

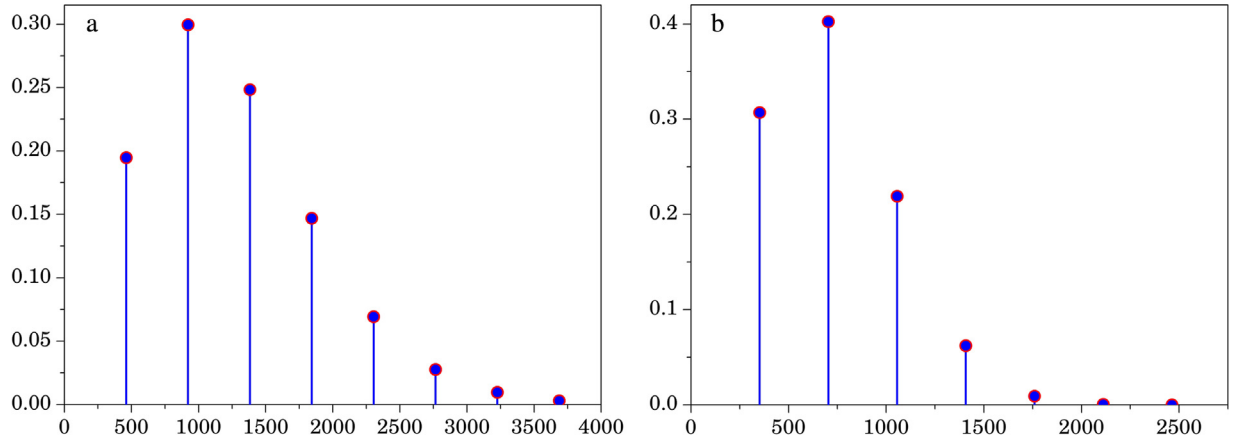

Figure 3. NEVPT2 Franck–Condon factor simulations for the $^7A_1$ ($^7\Sigma^+$) → $^6A_1$ ($^6\Sigma^+$) (a) and $^7A_1$ ($^7\Sigma^+$) → $^6B_1$ ($^6\Pi$) (b) transitions. Abscissa: vibrational transitions in wavenumbers; ordinate: intensities in arbitrary units. (a) $^7A_1$ ($^7\Sigma^+$) → $^6A_1$ ($^6\Sigma^+$); (b) $^7A_1$ ($^7\Sigma^+$) → $^6B_1$ ($^6\Pi$).

a maximal value of 45% in the case of the $^5B_1$ ($^5\Pi$) state, reflecting the maximal multi-reference character for this state.

3.3. Photoelectron spectrum of MnS^-

The photoelectron spectrum of MnS^- was measured with a photon energy of 355 nm or 3.49 eV [10]. In this spectrum, two bands with vertical detachment energies of 2.03 eV (X band) and 2.78 eV (A band) were observed. Also, the adiabatic detachment energy for the X band or the electron affinity of the neutral cluster was determined to be 1.77 eV, as the onset of this band. It should be noted that both these two features in the spectrum are broad bands with unresolved vibrational progressions, resulting from the usage of a laser beam of high energy (3.49 eV) photons to detach electrons from the anion. This implies that there should be a large difference between the Mn–S bond distance of the anionic ground state and that of the neutral ground state, and the involved yet undermined low-lying excited state.

In the present study, the NEVPT2 results are the only data that can safely be employed for the assignment of the photoelectron spectrum of MnS^-. Firstly, of all computational techniques considered it is the only one that can calculate all possible low-lying states. Secondly, it is the only multi-reference method which ensures that all states are treated at an equal level. Since the $^7A_1$ ($^7\Sigma^+$) is calculated as the anionic ground state, it should be considered as the initial state for the electron detachments. The ionization from the $^7\Sigma^+$ to the neutral $^6A_1$ ($^6\Sigma^+$) ground state, corresponding to the removal of an electron from the σ(4s,4p) orbital, is assigned to the X band. It should be noted that the adiabatic and vertical detachment energies (ADEs and VDEs) are respectively specified as adiabatic and vertical relative energies (AREs and VREs) in Table 1. For the $^7\Sigma^+ \rightarrow {}^6\Sigma^+$ transition, the ADE and VDE as calculated at NEVPT2 with AS I are 1.57 and 1.67 eV. With AS II, these values are improved to 1.63 and 1.75 eV, which compares well with experimental values of 1.77 eV and 2.03 eV. RCCSD(T) renders an adiabatic detachment energy value of 1.96 eV as can be seen in the lower part of Table 2, a value that is slightly higher than experiment. Further, the A band at 2.78 eV is proposed to be the result of the detachment of an electron from one of the d_π orbitals of the anionic ground state to create the first excited $^6B_1$ ($^6\Pi$) state of the neutral cluster. The NEVPT2 vertical detachment energies as calculated with the two employed active spaces are 2.58 eV and 2.62 eV, which are in good agreement with the experimental value of 2.78 eV. These assignments stem to reason as the detachment from the highest metal orbital, because of its 4s,4p character, is expected to give rise to the X band. On the other hand, electron detachments from the most anti-bonding metal d orbitals $5b_1$ and $5b_2$ underlies the higher energy A band. Indeed, their π anti-bonding nature places them above the $12a_1$ orbital, which as a σ anti-bonding orbital, is stabilized by the higher lying 4s and 4p orbitals. This effectively reduces its anti-bonding nature as can be deduced from Figure 1.

The Franck–Condon factor simulations for the $^7A_1$ ($^7\Sigma^+$) → $^6A_1$ ($^6\Sigma^+$) and the $^7A_1$ ($^7\Sigma^+$) → $^6B_1$ ($^6\Pi$) electron detachment processes confirm the newly made assignments. These simulations are performed on the basis of harmonic vibrational analyses, which made use of the potential energy curves for the related states as depicted in Figure 2. The calculated Franck–Condon factors are represented in Figure 3. The obtained silhouettes allow to deduce that both these one-electron detachment processes show broad vibrational progressions. The vibrational frequency of 461 cm^{-1} as obtained for the $^6A_1$ ($^6\Sigma^+$) state is considerably larger than the value of 352 cm^{-1} for $^6B_1$ ($^6\Pi$). Also, this figure unquestionably demonstrates that the vibrational progression for the transition to $^6A_1$ ($^6\Sigma^+$) is much broader than that of the ionization to $^6B_1$ ($^6\Pi$). At the NEVPT2 level, this can be understood by the larger Mn–S bond length difference between the anionic $^7A_1$ ($^7\Sigma^+$) ground state (2.169 Å) and the neutral $^6A_1$ ($^6\Sigma^+$) ground state (2.038 Å) as compared to the neutral $^6B_1$ ($^6\Pi$) first excited state (2.264 Å). In general, the Franck–Condon factor simulations predict that the X band should definitely be much broader than the A band, a prediction that is confirmed by the photoelectron spectrum [10]. Unfortunately the resolution of the experimental spectrum is not high enough to observe separate peaks that could be compared to the Franck–Condon simulations of Figure 3. Therefore, this remains a challenge for future experimental work.

4. Conclusions

The electronic structures of $MnS^{-/0}$ have been investigated by DFT, RCCSD(T), and NEVPT2 methods. The results show that the anionic and neutral ground states are $^7A_1$ ($^7\Sigma^+$) and $^6A_1$ ($^6\Sigma^+$), respectively. Therefore, the anion photoelectron spectrum of MnS^- is explained by using the $^7A_1$ ($^7\Sigma^+$) as the initial state for the two experimentally observed electron detachment processes. The X band is assigned to the $^7A_1$ ($^7\Sigma^+$) → $^6A_1$ ($^6\Sigma^+$) transition, corresponding to the removal of an electron from the predominantly 4s,4p orbital of manganese. The ADE and VDE of this transition as calculated at the NEVPT2 level are 1.63 eV and 1.75 eV, which compare well with the experimental values of 1.77 and 2.03 eV, respectively. The A band is ascribed to the $^7A_1$ ($^7\Sigma^+$) → $^6B_1$ ($^6\Pi$) transition, as the outcome of a one-electron detachment from the predominantly metal d_π anti-bonding orbitals. The vertical

detachment energy calculated at NEVPT2 level for this transition is 2.62 eV, which is in good agreement with the experimental value of 2.78 eV. The Franck–Condon factor simulations for the $^7A_1$ ($^7\Sigma^+$) → $^6A_1$ ($^6\Sigma^+$) and $^7A_1$ ($^7\Sigma^+$) → $^6B_1$ ($^6\Pi$) ionizations confirm the relative broadness of the X and A bands in the photoelectron spectrum of MnS^-.

References

[1] I. Stiefel Edward, Transition Metal Sulfur Chemistry, American Chemical Society, 1996, pp. 2.
[2] S. Harris, R.R. Chianelli, J. Catal. 86 (1984) 400.
[3] B. Liang, L. Andrews, J. Phys. Chem. A 106 (2002) 6295.
[4] B. Liang, L. Andrews, J. Phys. Chem. A 106 (2002) 6945.
[5] B. Liang, L. Andrews, J. Phys. Chem. A 106 (2002) 3738.
[6] B. Liang, X. Wang, L. Andrews, J. Phys. Chem. A 113 (2009) 3336.
[7] B. Liang, X. Wang, L. Andrews, J. Phys. Chem. A 113 (2009) 5375.
[8] H.-J. Zhai, B. Kiran, L.-S. Wang, J. Phys. Chem. A 107 (2003) 2821.
[9] N. Zhang, T. Hayase, H. Kawamata, K. Nakao, A. Nakajima, K. Kaya, J. Chem. Phys. 104 (1996) 3413.
[10] N. Zhang, H. Kawamata, A. Nakajima, K. Kaya, J. Chem. Phys. 104 (1996) 36.
[11] S. Clima, M.F.A. Hendrickx, J. Phys. Chem. A 111 (2007) 10988.
[12] S. Clima, M.F.A. Hendrickx, Chem. Phys. Lett. 436 (2007) 341.
[13] V.T. Tran, M.F.A. Hendrickx, J. Phys. Chem. A 115 (2011) 13956.
[14] V.T. Tran, M.F.A. Hendrickx, J. Phys. Chem. A 117 (2013) 3227.
[15] I.G. Dance, K.J. Fisher, Dalton Trans. (1997) 2563.
[16] Y.-C. Zhao, J. Yuan, Z.-G. Zhang, H.-G. Xu, W. Zheng, Dalton Trans. 40 (2011) 2502.
[17] C. Bauschlicher Jr., P. Maitre, Theor. Chim. Acta 90 (1995) 189.
[18] C. Angeli, R. Cimiraglia, S. Evangelisti, T. Leininger, J.-P. Malrieu, J. Chem. Phys. 114 (2001) 10252.
[19] C. Angeli, R. Cimiraglia, J.-P. Malrieu, Chem. Phys. Lett. 350 (2001) 297.
[20] C. Angeli, R. Cimiraglia, J.-P. Malrieu, J. Chem. Phys. 117 (2002) 9138.
[21] I. Schapiro, K. Sivalingam, F. Neese, J. Chem. Theory Comput. 9 (2013) 3567.
[22] C. Angeli, R. Cimiraglia, Mol. Phys. 109 (2011) 1503.
[23] M. Atanasov, P. Comba, S. Helmle, D. Müller, F. Neese, Inorg. Chem. 51 (2012) 12324.
[24] M. Atanasov, J.M. Zadrozny, J.R. Long, F. Neese, Chem. Sci. 4 (2013) 139.
[25] C. Camacho, H.A. Witek, R. Cimiraglia, J. Chem. Phys. 132 (2010) 244306.
[26] A. Domingo, M. Carvajal, C. Graaf, K. Sivalingam, F. Neese, C. Angeli, Theor. Chem. Acc. 131 (2012) 1.
[27] F. Neese, WIREs Comput. Mol. Sci. 2 (2012) 73.
[28] A.D. Becke, Phys. Rev. A 38 (1988) 3098.
[29] J.P. Perdew, Phys. Rev. B 33 (1986) 8822.
[30] A.D. Becke, J. Chem. Phys. 98 (1993) 5648.
[31] C. Lee, W. Yang, R.G. Parr, Phys. Rev. B 37 (1988) 785.
[32] F. Weigend, F. Furche, R. Ahlrichs, J. Chem. Phys. 119 (2003) 12753.
[33] H.-J. Werner, P.J. Knowles, F.R. Manby, M. Schütz, et al., MOLPRO, Version 1, A Package of Ab Initio Programs, 2009, see http://www.molpro.net
[34] N.B. Balabanov, K.A. Peterson, J. Chem. Phys. 123 (2005) 064107.
[35] R.A. Kendall, T.H. Dunning, R.J. Harrison, J. Chem. Phys. 96 (1992) 6796.
[36] Dalton, A Molecular Electronic Structure Program, Release DALTON2013.0, 2013, see http://daltonprogram.org/
[37] K. Aidas, C. Angeli, K.L. Bak, V. Bakken, R. Bast, L. Boman, O. Christiansen, R. Cimiraglia, S. Coriani, P. Dahle, E.K. Dalskov, U. Ekström, T. Enevoldsen, J.J. Eriksen, P. Ettenhuber, B. Fernández, L. Ferrighi, H. Fliegl, L. Frediani, K. Hald, A. Halkier, C. Hättig, H. Heiberg, T. Helgaker, A.C. Hennum, H. Hettema, E. Hjertenæs, S. Høst, I.-M. Høyvik, M.F. Iozzi, B. Jansík, H.J.A. Jensen, D. Jonsson, P. Jørgensen, J. Kauczor, S. Kirpekar, T. Kjærgaard, W. Klopper, S. Knecht, R. Kobayashi, H. Koch, J. Kongsted, A. Krapp, K. Kristensen, A. Ligabue, O.B. Lutnæs, J.I. Melo, K.V. Mikkelsen, R.H. Myhre, C. Neiss, C.B. Nielsen, P. Norman, J. Olsen, J.M.H. Olsen, A. Osted, M.J. Packer, F. Pawlowski, T.B. Pedersen, P.F. Provasi, S. Reine, Z. Rinkevicius, T.A. Ruden, K. Ruud, V.V. Rybkin, P. Sałek, C.C.M. Samson, A.S. de Merás, T. Saue, S.P.A. Sauer, B. Schimmelpfennig, K. Sneskov, A.H. Steindal, K.O. Sylvester-Hvid, P.R. Taylor, A.M. Teale, E.I. Tellgren, D.P. Tew, A.J. Thorvaldsen, L. Thøgersen, O. Vahtras, M.A. Watson, D.J.D. Wilson, M. Ziolkowski, H. Ågren, WIREs Comput. Mol. Sci. 4 (2014) 269.
[38] Y. Ishikawa, M.J. Vilkas, J. Mol. Struct.: THEOCHEM 573 (2001) 139.
[39] M. Reiher, A. Wolf, J. Chem. Phys. 121 (2004) 10945.
[40] M. Reiher, A. Wolf, J. Chem. Phys. 121 (2004) 2037.
[41] M.F.A. Hendrickx, K.R. Anam, J. Phys. Chem. A 113 (2009) 8746.